The Effects of Carbidopa Administration on 6-[^{18}F]Fluoro-L-DOPA Kinetics in Positron Emission Tomography

John M. Hoffman,* William P. Melega, Thomas C. Hawk, Scott C. Grafton, Andre Luxen,† D. Kirk Mahoney, Jorge R. Barrio, Sung-Cheng Huang, John C. Mazziotta, and Michael E. Phelps

Division of Nuclear Medicine and Biophysics, Departments of Radiological Sciences, Pharmacology and Neurology and Laboratory of Nuclear Medicine, Laboratory of Biomedical and Environmental Sciences, UCLA School of Medicine, University of California at Los Angeles, Los Angeles, California

Carbidopa (L-α-hydrazino-α-methyl-b-(3,4-dihydroxyphenyl) propionic acid is a known inhibitor of aromatic amino acid decarboxylase. In both humans and monkeys, we studied the effects of carbidopa on plasma and brain kinetics of 6-[^{18}F] fluoro-L-DOPA (FDOPA), an analog of L-DOPA used for PET studies of the central dopaminergic system. Pretreatment with carbidopa resulted in increases in the plasma levels of FDOPA and 3-O-methyl-6-[^{18}F]fluoro-L-DOPA (3-OMFD). Total striatal and cerebellar activities measured with PET were also increased. Furthermore, increases observed in the specific striatal activity (striatum minus cerebellum total activity) were correlated with increases in the plasma FDOPA curve. Carbidopa pretreatment did not affect the influx rate constant (K) for FDOPA from plasma to striatum in humans as determined by Patlak graphical analysis. Thus, an increase in measured striatal tomographic activity was secondary to the increase in plasma FDOPA levels rather than as a result of changes in the FDOPA influx rate constant.

J Nucl Med 1992; 33:1472–1477

Carbidopa, an inhibitor of aromatic amino acid decarboxylase, is known to inhibit the conversion of L-DOPA to dopamine in extracerebral tissues (*1,2*). In humans, a major portion of orally administered L-DOPA is decarboxylated in the gastrointestinal tract (*3,4*) and in brain capillary endothelium (*5–7*). Therefore, the use of carbidopa in combination with L-DOPA (Sinemet®) therapy constitutes an effective mechanism to increase the bioavailability of L-DOPA administration in patients.

6-[^{18}F]fluoro-L-DOPA (FDOPA), a positron-emitting analog of L-DOPA, has been used to evaluate the integrity of the central dopaminergic system using positron emission tomography (PET) (*8–12*). Carbidopa pretreatment has been included in some FDOPA-PET studies (*13–16*), but its effects on FDOPA kinetics have not been analyzed. The present work evaluates the effects of carbidopa on striatal FDOPA kinetics with PET in both monkeys and humans.

METHODS

Synthesis Methods

FDOPA was prepared using the radiofluorodemercuration procedure previously described (*17–19*). The injected product had a radiochemical purity greater than 99% with a specific activity of 1–2 Ci/mmol. The compound was sterile and pyrogen-free.

Carbidopa Administration

For studies in monkeys (Macaca nemestrina weighing 5–7 kg, both sexes), carbidopa (provided by Merck, Sharp, and Dohme, Westpoint, PA) (5 mg/kg; i.v.,) was administrated 60 min prior to injection of FDOPA. Two monkeys did not receive carbidopa and were used as controls. For human studies, subjects were divided into one control group (n = 3) and two carbidopa pretreatments (p.o): 100 mg (n = 4), or 250 mg, (n = 3).

Nonhuman Primate Studies

Monkeys were deprived of food and liquids from midnight prior to the PET study; otherwise they were fed food and water ad libitum as per UCLA animal science guidelines. Initial anesthetization was performed with 100–150 mg ketamine (i.m.) followed by administration of 25–50 mg of pentobarbital (i.v.). Intratracheal intubation was then performed and the animal was maintained on a neonatal ventilator. A distal lower extremity artery was isolated and, with lidocaine injection, a cutdown was performed to allow cannulation of the femoral artery with a teflon catheter. All animals were administered pentobarbital (approximately 25 mg every 1–2 hr) to maintain adequate anesthesia as judged by monitoring of blood pressure, movement, and corneal responses. Body temperature was maintained with a heating blanket. Arterial blood gases, hematocrit, and serum glucose were also monitored throughout the course of each study. To initiate the study, FDOPA (1.1–5.1 mCi) was administered as a bolus injection via the venous catheter.

Received Oct. 2, 1991; revision accepted Mar. 19, 1992.

For reprints contact: * John M. Hoffman, Section of Nuclear Medicine, Department of Radiology, Box 3808, Duke University Medical Center, Durham, NC 27710.

* Current address: Section of Nuclear Medicine, Department of Radiology, Box 3808, Duke University Medical Center, Durham, NC 27710.

† Current address: Cliniques Universitaire, De Bruxelles, Hospital Erasme, Route De Lennik 808, B-1070 Bruxelles, Belgium.

Human Studies

Ten normal male volunteers (20–30 yr of age) were studied after their informed consent was obtained in accordance with the UCLA Human Subject Protection Committee. All subjects were fasted 4 hr prior to the study. Radial artery and venous catheterization were performed and then FDOPA (2.3–10.0 mCi) was administered as a bolus via the venous catheter.

Tomographic Imaging

PET studies were performed using the ECAT 831 tomograph (Siemens, Knoxville, TN). This particular tomograph permits simultaneous acquisition of 15 axial sections with a center-to-center separation of 6.4 mm. All studies were reconstructed with a Hanning filter (cutoff frequency = Nyquist frequency) resulting in image resolution of 8.5 × 8.5 × 7.0 mm (FWHM). The monkeys were positioned supine with the head inclined 18° (tilted inferiorly) relative to the orbito-meatal line. Humans were positioned supine with the imaging plane parallel to the orbito-meatal line. During the scanning procedure, the monkeys were anesthesized (see above) and their head fixed in position with foam pillows. For human subjects, head placement was maintained by foam pillows and velcro strap restraints. A transmission scan with ^{68}Ge ring source was performed for correction of attenuation (*20*). After administration of FDOPA, sequential emission scans were obtained beginning immediately after tracer administration using the following scanning sequence for monkeys: ten 90-sec images, nine 5-min images, six 10-min images. The scanning sequence for the human studies was: six 30-sec scans, four 3-min scans, five 10-min scans and three 20-min scans.

Rapid arterial blood sampling was performed via the indwelling radial artery catheter in the human subjects and via the femoral artery catheter in monkeys. Whole blood samples (2.0 ml each for humans, 0.25 ml each for monkeys) were taken using the following protocol: twelve samples at 10-sec intervals for 2 min beginning immediately after tracer injection, and additionally at 3, 4, 5, 7, 10, 30, 60 and 120 min. Plasma metabolite determination was performed on samples drawn at 5, 10, 30, 60 and 120 min after tracer injection. Samples were centrifuged, the plasma was separated and the activity was measured in a well counter to provide the ^{18}F arterial time-activity curve.

FDOPA Metabolites in Plasma

FDOPA and its metabolites were analyzed in the plasma of both monkeys and human subjects by high pressure liquid chromatography as previously described (*15*). The corrected plasma FDOPA arterial input function was then generated from the ^{18}F time-activity curve and the percentage of FDOPA and its metabolites at 5, 10, 30, 60 and 120 min (data not shown) (*21*). Calibration between the tomograph and well counter was established using a ^{18}F uniform cylinder so that plasma activity and regional brain activity could be expressed in the same units of cps/ml.

DATA ANALYSIS

Region of Interest Analysis. Regions of interest (ROIs) were drawn on the reconstructed PET images to define the striatal (caudate and putamen) and cerebellar regions bilaterally (*21*). ROIs (~4–5 cm^2 in area on a cross-sectional plane of largest striatal area) were defined separately according to the apparent boundary of the structure on the emission images for the left and right striata, based on a summed image from 60–120 min. ROIs (~10 cm^2 in area) for the cerebellar hemispheres were similarly drawn, but were based on early images (1–10 min). Those ROIs were then applied to the serial PET images obtained at various scan times and corrected for radioactive decay to give tissue ^{18}F time-activity curves of the corresponding regions. The curves from the left and the right sides were averaged to give a single striatal and a single cerebellar curve for each study. These curves were also normalized for the injected FDOPA dose in mCi/kg.

In small structures such as the striatum, ROI analysis can produce partial volume effects. With the ROIs and the imaging resolution used in this study, the ROI values would have approximately a 40% underestimation of the true radioactivity concentration in striatum (*22*). This underestimation, however, occurred in all studies and thus would not affect results unique to the carbidopa pretreatment.

Graphical Analysis. FDOPA tissue-time activity data were analyzed using the graphical technique as described by Patlak et al. (*23,24*). This technique is effective when the tracer is metabolically trapped in tissue (25); for FDOPA, its conversion to 6-[^{18}F]-fluorodopamine (FDA) is considered irreversible in normal brain and is followed by the trapping of FDA within neuronal vesicles; minimal clearance of the tracer is observed during the experimental period (*21,26–28*). The major peripheral metabolite of FDOPA, 3-O-methyl-6-[^{18}F]fluoro-L-DOPA (3-OMFD), is also transported into the brain. However, since 3-OMFD distribution appears to be uniform in brain tissue (*29*), the subtraction of cerebellar activity (which contains primarily 3-OMFD at later scan times) from striatal activity can be used to eliminate the contribution due to 3-OMFD. The results will then represent specific uptake of FDOPA in the striatum. The Patlak equation can be rewritten as:

$$[S(T) - C(T)]/Cp(T) = K \int_0^T Cp(t)\,dt/Cp(T) - B,$$

where S(T)-C(T) represents the specific striatal activity at time T, Cp(T) is the concentration of FDOPA in plasma at time T, K is the influx rate constant of FDOPA from plasma to striatum and B is a constant related to the distribution volume of FDOPA in striatum. When [S(T)-C(T)]/Cp(T) is plotted against the integral from time O to T of Cp(t)/Cp(T), the resultant curve should asymptotically approach a straight line with a slope (in units of

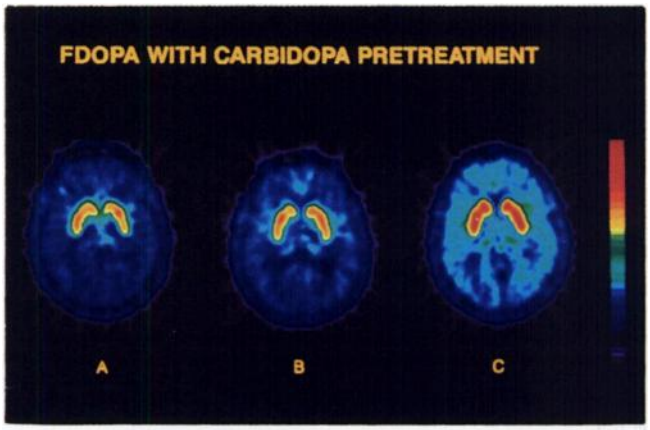

FIGURE 1. FDOPA-PET summed images (60–120 min) for three individuals pretreated with carbidopa: (A) 0 mg, (B) 100 mg, (C) 250 mg at 60 min prior to the FDOPA injection. All images are expressed as (counts/s)/g and are normalized by injected dose in mCi/kg.

ml/(g • min)) equal to the influx rate constant of FDOPA from the plasma to the striatum. Linear regression analysis was used to fit the data (from 15 to 120 min) to give the estimates of K and B.

RESULTS

After FDOPA administration, radioactivity progressively accumulated in the striatum of both normal monkeys and humans. By 2 hr after injection, activity in the striatum was very prominent when compared with background activity noted in the cerebellum. Figure 1 depicts summed human images (60–120 min) of tracer distribution cps after FDOPA injection into a representative subject from each group (0, 100, 250 mg carbidopa) normalized by injected dose in mCi/kg. The figure shows increases in striatal uptake with increases in administered carbidopa dose.

The effects of carbidopa pretreatment on tissue-time activity curves for the striatum and cerebellum in humans and in monkeys are shown in Figure 2. After tracer injection, a similar pattern of progressive accumulation of activity was observed that peaked at 30–40 min for the striatum and at 10–20 min for the cerebellum.

Figure 3 shows the relationship between the administered carbidopa dose and the measured radioactivity levels in plasma and in tissue. In Figure 3A, the areas under both the plasma FDOPA curve and the 3-OMFD curve from 0 to 120 min were increased with larger doses of carbidopa (correlation coefficient, r = 0.86 and 0.81, respectively). Figure 3B shows that the total radioactivity levels in both striatum and cerebellum were also increased with carbidopa pretreatment (r = 0.81 and 0.80, respectively). Figure 4 shows a strong correlation (r = 0.84) between FDOPA uptake (total and specific) in the striatum and the area under the FDOPA plasma curve, indicating that the increase in tissue radioactivity is a result of increases in plasma levels following carbidopa pretreatment.

Table 1 summarizes the Patlak graphical analysis results for the human subjects. Included is the regressed slope and intercept. Analysis of variance was performed on the slope values for the 0 mg, 100 mg and 250 mg pretreated individuals. No significant difference was noted for the slope values among the three groups.

DISCUSSION

Carbidopa has become an important adjunct in the treatment of Parkinson's disease with L-DOPA (*30*). Initially, studies showed that L-DOPA bioavailability was increased with carbidopa pretreatment that effectively inhibited peripheral decarboxylase activity (*31*); improvements in motor function were attributed to resultant increases in dopamine brain levels (*32*). More recently, investigations have shown that increases in L-DOPA bioavailability are correlated with carbidopa dose (*30*).

FDOPA is being used to probe presynaptic dopaminergic mechanisms with PET in animals and humans (*33*). The use of FDOPA as an analog of L-DOPA with PET has been validated with double-label experiments (FDOPA

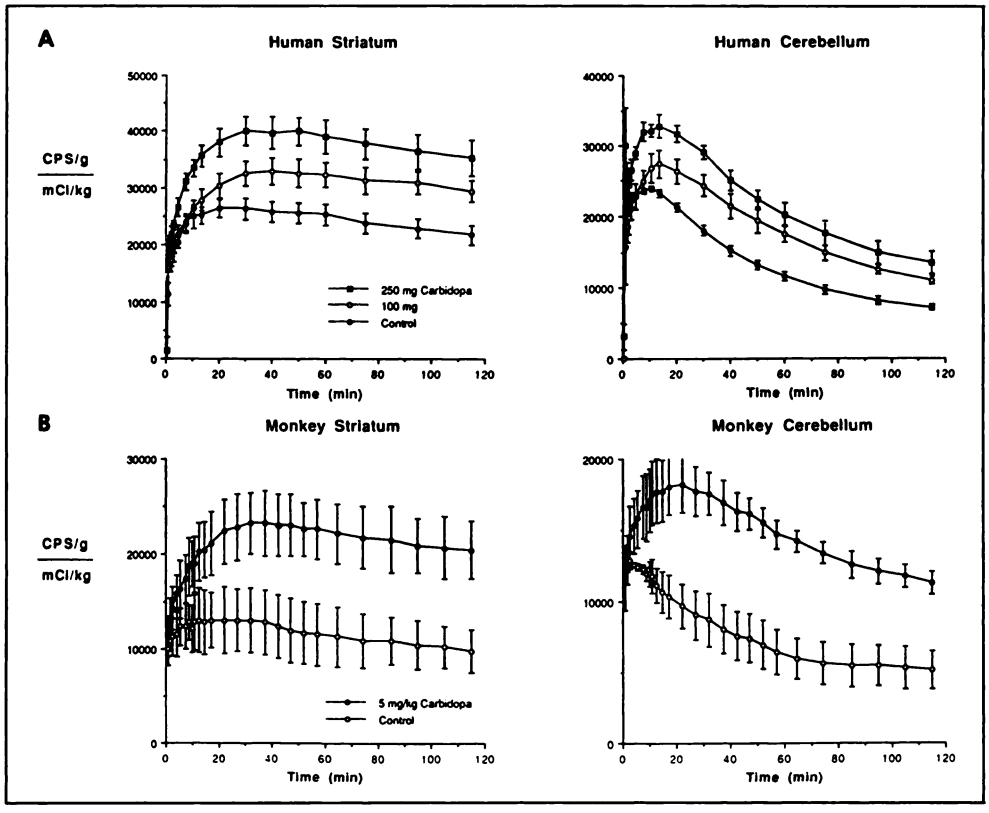

FIGURE 2. (A) Fluorine-18 tissue time-activity curves after FDOPA injection for human striatum and cerebellum. Carbidopa was administered at 60 min prior to the FDOPA injection: controls (n = 3; mean ± s.d.); 100 mg (n = 4; mean ± s.d.); 250 mg (n = 3; mean ± s.d.). (B) Fluorine-18 tissue time-activity curves after FDOPA injection for monkey striatum and cerebellum. Carbidopa (5 mg/kg, i.v.) was administered at 60 min prior to the FDOPA injection.

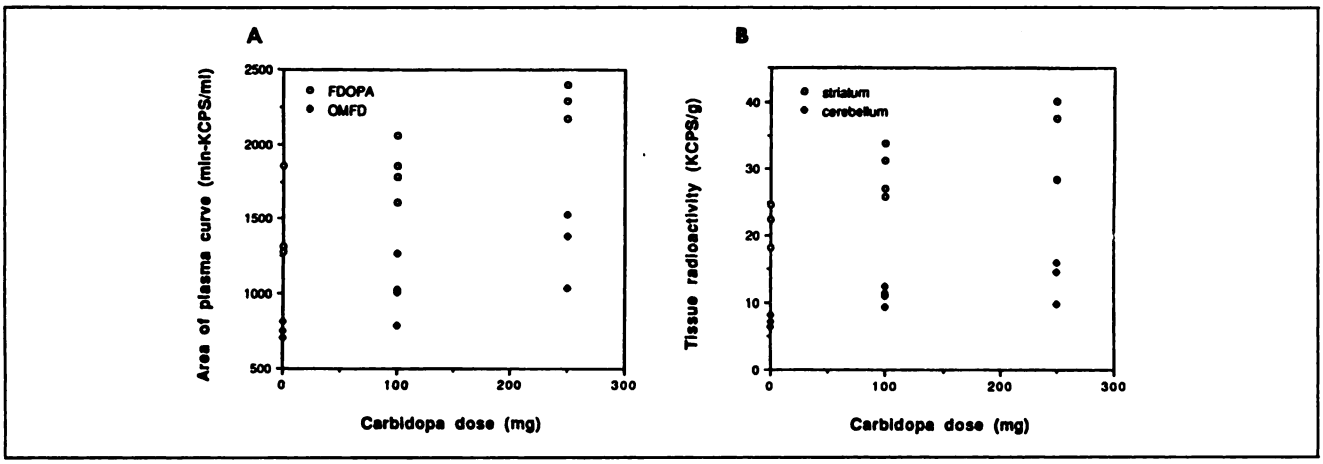

FIGURE 3. (A) Area under the curve for plasma FDOPA (O) and 3-OMFD (◆) versus administered carbidopa dose. Carbidopa (100 mg or 250 mg) was administered at 60 min prior to the FDOPA injection. Carbidopa plasma levels at the time of injection were 0.09 ± 0.04 μg/ml (n = 4; mean ± s.d.) for 100 mg and 0.19 ± 0.06 μg/ml (n = 3; mean ± s.d.) for 250 mg carbidopa administered. We have subsequently shown in humans that 200 mg carbidopa 90 min prior to the FDOPA injection are sufficient to restrict peripheral FDOPA metabolism to only 3-OMFD (11). (B) Total radioactivity area under the curve for striatum (O) and cerebellum (◆) as a function of carbidopa dose.

and [^{3}H]DOPA) in rats. These studies revealed markedly similar peripheral and central metabolism pathways for both tracers (*34*). It has also been shown that carbidopa pretreatment altered the peripheral metabolism of FDOPA, analogous to its effects on L-DOPA metabolism, such that increases in rat striatal FDA levels were observed (*15*). These particular findings became the impetus for our investigation on the effects of carbidopa on FDOPA kinetics and metabolism in PET studies.

We have now shown that for FDOPA-PET studies in monkeys and humans, FDOPA and 3-OMFD plasma levels (Fig. 3A) along with tomographic total activities in striatum and cerebellum are increased as a function of carbidopa dose (Figs. 1, 2 and 3B). Since 3-OMFD crosses the blood-brain barrier, the total activity measured by PET in striatal tissue includes 3-OMFD, in addition to FDOPA and its neuronal metabolites, FDA, 6-[^{18}F]fluoro-3,4-dihydroxyphenylacetic acid (FDOPAC) and 6-[^{18}F]fluorohomovanillic acid (FHVA) (*35,36*).

With carbidopa pretreatment, increases in tomographic striatal activity specific to dopaminergic processes are also correlated with FDOPA plasma levels. These changes, however, were only detected by the striatum-cerebellum subtraction method. No significant differences were observed in striatum-to-cerebellum (S/C) ratios with carbidopa dose; S/C = 3.0 with 0 mg, 2.7 with 100 mg, 2.7 with 250 mg carbidopa.

By using the techniques of Patlak et al. (*23,24*), we have demonstrated that pretreatment with carbidopa does not significantly affect the influx rate constant (K) for FDOPA

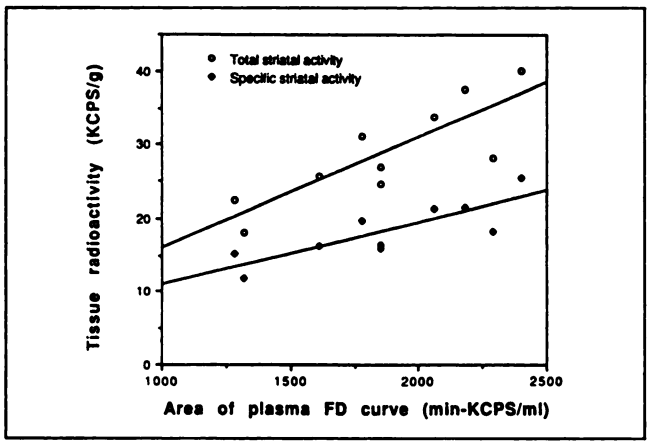

FIGURE 4. Total (O) and specific (◆) striatal activity versus area under the plasma FDOPA curve. The specific striatal activity was derived from striatum minus cerebellum total activity (see Figure 3 for methods).

TABLE 1
Graphical Analysis (Humans)

Subject no.	Carbidopa dose (mg)	Slope K (ml/min·g)	Intercept ml/g	Mean slope ± s.d.
1	0	0.009	−0.28	0.011 ± 0.002
2	0	0.013	−0.13	
3	0	0.010	−0.18	
4	100	0.009	−0.16	0.010 ± 0.002
5	100	0.008	−0.11	
6	100	0.010	−0.22	
7	100	0.012	−0.19	
8	250	0.008	−0.18	0.010 ± 0.002
9	250	0.010	−0.13	
10	250	0.011	−0.17	

Graphical analysis results using the Patlak method are shown. Included is the dosage of carbidopa, the regression fitted slope and the y-intercept. Analysis of variance was then performed between the slope values of each carbidopa administration scheme; the absence of any significant difference between the slopes indicates that carbidopa does not affect the FDOPA influx constant.

from the plasma to the striatum (Table 1). This confirms the notion that the increased striatal activity measured by PET is secondary to increases in FDOPA plasma levels rather than in an alteration in blood-brain barrier transport. The striatum-cerebellum subtraction method used for this analysis was derived from the striatum total activity minus cerebellum activity (nonspecific). In the cerebellum, an area essentially devoid of dopaminergic neurons, the tomographic activity represented nonspecific accumulation of 3-OMFD and FDOPA (*21,28*). By subtraction of cerebellar from total striatal activity at each time point of the tissue time-activity curve, specific striatal tracer accumulation was determined (*25*). Although studies in rodents have shown that the FDOPA level in the striatum is lower than that in the cerebellum (*15*), for these studies the oversubtraction of free FDOPA, as reflected in the striatum-cerebellum difference, would not affect the slope of the data in the Patlak graphical analysis because the free FDOPA component in tissue has a zero slope on the Patlak plot (*37*). Furthermore, the oversubtraction error was minimized at later scan times when the majority of activity was represented by 3-OMFD.

In conclusion, we have shown in this work that for FDOPA-PET studies carbidopa pretreatment increases total and specific brain tomographic activity per unit dose of FDOPA. Also, graphical analysis techniques reveal that the influx rate constant for FDOPA transport from plasma to striatum does not change. The resultant greater activity in brain structures for a given FDOPA dose provides lower statistical noise in the PET images and allows for a more accurate delineation of dopaminergic structures, especially in situations where their integrity is compromised (e.g., Parkinson's disease). Conversely, for multiple studies on a human subject, lower FDOPA doses can be used without compromising image quality, thus reducing unnecessary radiation exposure.

ACKNOWLEDGMENTS

The authors wish to thank the technical and support staff of the Division of Nuclear Medicine for their assistance in performing and analyzing the studies required to prepare this manuscript. We gratefully acknowledge the gift of carbidopa from Merck, Sharpe, and Dohme Ltd. This research was supported by Department of Energy (DOE) contract DE-AC03 76-SF00012 and NIH grants, NS15654 and MH37916.

REFERENCES

1. Jaffe M. Clinical studies of carbidopa and L-DOPA in the treatment of Parkinson's disease. *Adv Neurol* 1973;2:161–172.
2. Pinder RM, Brogden RN, Sawyer PW, et al. Levodopa and decarboxylase inhibitors: a review of their clinical pharmacology and use in the treatment of parkinsonism. *Drugs* 1976;11:324–377.
3. Andersson I, Granerus A-K, Jagenburb R, et al. Intestinal decarboxylation of orally administered L-DOPA. *Acta Med Scand* 1975;198:415–420.
4. Nutt JG, Woodward WR, Anderson WL, et al. What is the function of carbidopa in the treatment of Parkinsonism? *Ann Neurol* 1983;14: 133–134.
5. Lloyd K, Hornykiewicz O. Parkinson's disease: activity of L-DOPA decarboxylase in discrete brain regions. *Science* 1970;170:1212–1213.
6. Hardebo JE, Owman C. Barrier mechanisms for neurotransmitter monoamines and their precursors in the blood-brain interface. *Ann Neurol* 1980; 8:1–11.
7. Hardebo JE, Ernson PC, Falck B, et al. Enzymes related to monoamine transmitter metabolism in brain microvessels. *J Neurochem* 1980;35: 1388–1393.
8. Garnett ES, Firnau G, Nahmias C, et al. Striatal dopamine metabolism in living monkeys examined by positron emission tomography. *Brain Res* 1983;280:169–171.
9. Garnett ES, Firnau G, Nahmias C. Dopamine visualized in the basal ganglia of living man. *Nature* 1983;305:137–138.
10. Garnett ES, Firnau G, Nahmias C, et al. Blood-brain barrier transport and cerebral utilization of dopa in living monkeys. *Am J Physiol* 1980;238: 318–327.
11. Melega WP, Grafton SC, Huang SC, et al. 6-[^{18}F]Fluoro-L-DOPA metabolism in monkeys and humans: biochemical parameters for the formulation of tracer kinetic models with positron emission tomography. *J Cereb Blood Flow Metab* 1991;11:890–897.
12. Hoffman JM, Grafton SC, Melega WP, et al. Characterization of 6-[^{18}F] fluoro-L-DOPA (FD) as a probe of striatal pre-synaptic dopaminergic function. *Neurology* 1989;39:(suppl 1):164.
13. Hoffman JM, Melega WP, Grafton ST, et al. The importance of carbidopa in 6-^{18}F-fluoro-L-DOPA (FD) PET studies. *J Nucl Med* 1989;30:761.
14. Melega WP, Hoffman JM, Luxen A, et al. Effects of carbidopa on the peripheral and cerebral 6-[^{18}F] fluoro-L-DOPA metabolism in monkeys and humans; tracer kinetic correlates for positron emission tomography. *Proc Internat Symp Cereb Blood Flow Metab* 1989;9(suppl 1):S420.
15. Melega WP, Hoffman JM, Luxen A, et al. The effects of carbidopa on the metabolism of 6-[^{18}F]-fluoro-L-DOPA in rats, monkeys, and humans. *Life Sci* 1990;47:149–157.
16. Boyes BE, Cumming P, Martin WRW, et al. Determination of plasma [^{18}F]-6-fluorodopa during positron emission tomography: elimination and metabolism in carbidopa treated subjects. *Life Sci* 1986;39:2243–2252.
17. Luxen A, Barrio JR, Bida GT, et al. Regioselective radiofluorodemurcuration: a simple high yield synthesis of 6-[^{18}F] fluoro-L-DOPA. *J Lab Comp Radiopharm* 1986;23:1066.
18. Luxen A, Hoffman JM, Bida GT, et al. Metabolism of 6-[F-18]-fluoro-L-DOPA in rodents and primates. *Proc Internat Symp Cerebral Blood Flow Metab* 1987;7(suppl):S362.
19. Luxen A, Barrio JR. Fluorination of substituted veratroles via regioselective mercuration. *Tetrahedron Letters* 1988;29:1501–1054.
20. Huang SC, Hoffman EJ, Phelps ME, et al. Quantitation in positron emission computer tomography: 2. Effects on inaccurate attenuation connection. *J Comput Assist Tomogr* 1979;3:804–814.
21. Huang SC, Yu DC, Barrio JR, et al. Kinetics and modeling of 6-[F-18] fluoro-L-DOPA in human positron emission tomographic studies. *J Cereb Blood Flow Metab* 1991;11:898–913.
22. Huang SC, Yu DC, Grafton S, et al. Effects of ROI size on determination of striatal 6-[^{18}F]fluoro-L-DOPA kinetics in PET studies. *J Cereb Blood Flow Metab* 1991;2(suppl 2):S158.
23. Patlak CS, Blasberg RG, Fenstermacher JD. Graphical evaluation of blood to brain transfer constants from multiple time uptake data. *J Cereb Blood Flow Metab* 1983;3:1–7.
24. Patlak CS, Blasberg RG. Graphical evaluation of blood to brain transfer constants from multiple time uptake data: generalizations. *J Cereb Blood Flow Metab* 1985;5:584–590.
25. Martin WRW, Palmer MR, Patlak CS, et al. Nigrostriatal function in humans studies with positron emission tomography. *Ann Neurol* 1989;26: 535–542.
26. Barrio JR, Huang SC, Melega WP, et al. 6-[^{18}F]Fluoro-L-DOPA probes dopamine turnover rates in central dopaminergic structures. *J Neurosci Res* 1990;27:487–493.
27. Melega WP, Hoffman JM, Schneider JS, et al. 6-[^{18}F] Fluoro-L-DOPA metabolism in MPTP-treated monkeys: assessment of tracer methodologies for positron emission tomography. *Brain Res* 1991;543:271–276.
28. Huang SC, Barrio JR, Hoffman JM, et al. A compartmental model for 6-[F-18] fluoro-L-DOPA kinetics in cerebral tissues. *J Nucl Med* 1989;30: 735.
29. Doudet DJ, McLellan CA, Carson R, et al. Distribution and kinetics of 3-O-methyl-6-[F-18]fluoro-L-DOPA in the rhesus monkey brain. *J Cereb Blood Flow Metab* 1991;11:726–734.
30. Cedarbaum JM, Kuty H, Dhar AK, et al. Effect of supplemental carbidopa on bioavailability of L-DOPA. *Clin Neuropharmacol* 1986;9:153–159.
31. Porter CC, Watson LS, Titus DC, et al. Inhibition of DOPA decarboxylase by the hydrazino analog of L-alpha-methyldopa. *Biochem Pharmacol* 1962;

11:1067–1077.
32. Lotti VJ, Porter CC. Potentiation and inhibition of some central actions of L(−) dopa by decarboxylase inhibitors. *J Pharmacol Exp Ther* 1970; 172:406–415.
33. Barrio JR. Approaches to the design of biochemical probes for positron emission tomography. *Neurochem Res* 1991;16:1047–1054.
34. Melega WP, Luxen A, Perlmutter MM, et al. Comparative in-vivo metabolism of 6-[^{18}F]fluoro-L-DOPA and [^{3}H]L-Dopa in rats. *Biochem Pharmacol* 1990;39:1853–1860.
35. Chiueh CC, Kirk KL, Channing MA, et al. Neurochemical basis for the use of 6-FDOPA for visualizing dopamine neurons in the brain by positron emission tomography. *Soc Neurosci Abstrs* 1984;14:883.
36. Chiueh CC, Zukowska-Grojec Z, Kirk KL, et al. 6-Fluorocatecholamines as false adrenergic neurotransmitter. *J Pharmacol Exp Ther* 1983;225: 529–533.
37. Choi Y, Hawkins RA, Huang SC, et al. Parametric images of myocardial metabolic rate of glucose generated from dynamic cardiac PET and 2-[^{18}F] fluoro-2-deoxy-d-glucose studies. *J Nucl Med* 1991;32:733–738.

(continued from page 1443)

SELF-STUDY TEST
Radiobiology and Radiation Protection

Questions are taken from the *Nuclear Medicine Self-Study Program I,* published by The Society of Nuclear Medicine

19. a balancing of ^{131}I hazard vs. risk of ^{127}I.
20. federal regulations for emergency situations.

Patients are rushed to the emergency room of your hospital after an accident at a nuclear reactor site. Concerning the care of patients potentially contaminated with radionuclides,

21. the JCAHO requires all accredited hospitals to have written plans for the care of such casualties.
22. steps must be taken immediately to interrupt any radiation-induced injury process.
23. the patient, even if critically injured, should be kept in the ambulance until a radiation survey can be completed.
24. the patient should be washed and showered prior to treatment to remove as much contamination as possible.
25. a determination of the absolute lymphocyte count is essential.

SELF-STUDY TEST
Radiobiology and Radiation Protection
ANSWERS

ITEM 1-5: Sources of Radiation Exposure
ANSWERS: 1, A; 2, C; 3, E; 4, D; 5, D
The sources of radiation dose received by the U.S. population have been summarized by a number of national and international bodies. The estimates vary slightly between agencies, but the estimates given below from the National Academy of Sciences, BEIR Committee (1980), represent an average of these values.

U.S. General Population Exposure Estimates

Source	Average Individual Dose (mrem/year)	%	Ratio of Source$_i$: Natural Background
Natural background	82	44	1:1
Medical x-rays, 79 mrem/year radiopharmaceuticals, 14 mrem/year	93	50	1:1
Fallout	4–5	2.4	1:20
Consumer products	3–4	1.9	1:20
Nuclear industry	<1	<0.5	1:80
Airline travel	0.6	0.3	1:130
Total	≅185	≅100	

Note added in proof: Recently, the NCRP has reevaluated radiation exposure in the U.S. (NCRP Report No. 93, *Ionizing Radiation Exposure of the Population of the United States.* 1987.) This new assessment of the average exposure of the members of the U.S. population to all sources of ionizing radiation is the first based upon a common unit, the effective dose equivalent (which weighs the risks of partial-body irradiation). The average annual effective dose equivalent to individuals in the U.S. population is 360 mrem (3.6 mSv). The major part of this, 300 mrem (3 mSv), is from background which includes 200 mrem (2 mSv) from radon and its decay products. The relative contribution of medical diagnosis, which amounts to 54 mrem (39 mrem from x-ray examinations and 14 mrem from radiopharmaceuticals), is less than that estimated in previous evaluations. This contribution, 15% of the total, is less than the 50% estimate of BEIR-1980 (93 mrem medical versus 185 mrem total).

ITEMS 6-9: Acute Radiation Syndromes
ANSWERS: 6, A; 7, B; 8, C; 9, E
About 2 hours after rapid exposure of all or a major portion of the body to high doses of radiation, humans begin to show signs and symptoms of acute gastrointestinal and neuromuscular effects, which are collectively called the prodromal syndrome. Its German designation *Strahlenkater* is compounded from "radiation" and "hangover," which its symptoms mimic. Nausea and vomiting begin at about 50 rads. The threshold for radiation-induced lethality in humans is about 200 rads. As dose levels rise above this, mortality increases. Humans appear to develop and recover from signs of hematologic damage more slowly than other mammals. The peak incidence of human deaths from hematologic damage occurs at about 30 days but deaths continue for up to 60 days, whereas the peak incidence of death in animals occurs at 10–15 days. Thus the lethal dose for 50% of an irradiated population, the LD_{50}, is best estimated for a period of 60 days in humans and 30 days in animals. The estimated $LD_{50/60}$ for humans is 350 rads. Seizure and coma occur only after total body doses on the order of 5000 rads.

References
1. Baverstock KF, Ash PJND. A review of radiation accidents involving whole body exposure and the relevance of the $LD_{50/60}$ for man. *Br J Radiol* 1983;56:837–849.
(continued on page 1500)